IJIE

INTERNATIONAL JOURNAL OF INTEGRATED ENGINEERING
ISSN: 2229-838X e-ISSN: 2600-7916

Vol. 18 No. 1 (2026) 72-83
https://publisher.uthm.edu.my/ojs/index.php/ijie

Characterization and Application of Na/SnO_2 Catalyst in Biodiesel Production: Insights into Structure and Performance

Feihu Zeng[1,2], SyYi Sim[3]*, Chen Xiaohua[1], Feng Wang[1], Lu Huangteng[4]

[1] *Light Industry College, Liming Vocation University, Quanzhou, 362000, CHINA*
[2] *Faculty of Engineering Technology, Universiti Tun Hussein Onn Malaysia, 84600, Pagoh, Johor, MALAYSIA*
[3] *Faculty of Electrical and Electronic Engineering, Universiti Tun Hussein Onn Malaysia, 86400, Johor, MALAYSIA*
[4] *Hubin Electrical Equipment Co., Ltd., Xiamen, 361000, CHINA*

*Corresponding Author: sysim@uthm.edu.my.
DOI: https://doi.org/10.30880/ijie.2026.18.01.006

Article Info

Received: 12 December 2025
Accepted: 28 March 2025
Available online: 17 April 2026

Keywords

Transesterification, solid bases, tin oxide, catalyst

Abstract

Biodiesel production via transesterification of rapeseed oils offers a sustainable substitute for fossil fuels, with solid base catalysts playing a key role in enhancing reaction efficiency. This study reports the synthesis a Na/SnO_2 solid base catalyst and its performance evaluation using the transesterification reaction of rapeseed oil. SnO_2 was synthesized via a precipitation method and subsequently combined with sodium metal under a nitrogen atmosphere. Sodium species interacted with SnO_2 through the formation of NaOH and Na_2O, bonding to surface hydroxyl groups or incorporating into lattice defects to generate strong basic sites (Hammett range: 11.2–15.6). Structural and surface properties were characterized by XRD, FT-IR, TG-DSC, SEM, and Hammett titration. Optimal catalytic performance was achieved under conditions of pH 8, calcination at 600°C for 3 hours, 0.015 mol surfactant concentration, and 3.75 wt.% sodium loading, yielding a biodiesel conversion rate of 93.6%. Results demonstrated that moderate calcination was critical to ensuring high crystalline and active site availability, while excessive thermal treatment induced sintering and deactivation. This work presents an innovative method to stabilize Na-based active sites and prevent SnO_2 dissolution, offering a viable route for designing high-performance solid superbases for green biodiesel synthesis.

1. Introduction

With the continuous advancement of industrialization, global energy consumption has increased rapidly, resulting in a growing dependence on fossil fuels. However, fossil energy sources are increasingly constrained by resource uncertainty and severe environmental impacts, prompting an urgent need for cleaner alternatives [1]. Biodiesel, a renewable, biodegradable, and environmentally friendly fuel primarily composed of fatty acid methyl esters, has

This is an open access article under the CC BY-NC-SA 4.0 license.

been widely recognized as a promising substitute for fossil fuels. Biodiesel generators can be used as a backup power source for renewable energy sources (e.g., wind power, tidal power) to provide supplemental power when the grid is unstable or there is a shortage of electrical energy [2]. The use of biodiesel as a sustainable energy storage source opens up possibilities for building miniaturized grid production facilities [3]. Biodiesel can be synthesized by transesterification [4] or esterification [5]. According to the American standard ASTM D6751, t Transesterification yields a higher fatty acid methyl ester content, ensuring the purity of fatty acid methyl esters in biodiesel (≥96.5%). Among the catalysts used to catalyze the transesterification reaction, alkali catalysts are favored due to their high reaction efficiency under mild conditions [6]. While homogeneous alkali catalysts (e.g., NaOH, KOH) provide fast reaction kinetics, they suffer from significant drawbacks including difficult separation, catalyst loss, and substantial wastewater generation, which hinder large-scale industrial adoption. Furthermore, the corrosive nature of homogeneous bases poses challenges for reactor materials and increases maintenance costs. Solid alkaline catalysts, as a subclass of heterogeneous systems, are increasingly utilized for their superior reusability and ease of separation. Within this category, monometallic oxides (e.g., CaO [7], MgO [8], ZrO_2 [9], TiO_2 [10]), molecular sieves [11], clay minerals [12], and alkali-loaded [13] carriers such as Na-ZrO_2 [14]and KOH/SnO_2 [15] have been extensively explored. SnO_2, in particular, has emerged as an effective support due to its inherent lattice defects [16] and Lewis acid centers [17][18], which enhance the dispersion and stability of alkaline active sites [19]. The presence of oxygen vacancies and acidic sites on SnO_2 not only facilitates alkali metal anchoring but may also promote reactant adsorption, thereby synergistically enhancing the transesterification process. However, conventional preparation methods for alkali-supported SnO_2 catalysts, often involving wet impregnation followed by high-temperature calcination, face notable challenges. These processes typically consume large quantities of alkali precursors and can induce partial dissolution of the SnO_2 support. This reaction forms soluble stannate species, which may compromise the structural integrity and long-term stability of the catalyst [15]. Therefore, developing a synthesis strategy that minimizes alkali usage while maximizing the structural stability of SnO_2-supported catalysts remains a critical research objective.

To address the aforementioned limitations, we herein report a novel strategy for the synthesis of Na/SnO_2 solid base catalysts. This approach involves an in-situ solid-state reaction between a SnO_2 precursor and a sodium source under controlled nitrogen atmosphere and temperature. The synthesis is designed to achieve stable Na incorporation through deliberate lattice defect engineering [20], with the dual objectives of minimizing alkali usage and enhancing the structural stability of the catalyst. The nitrogen atmosphere is crucial to prevent premature oxidation of metallic sodium and to control the reaction pathway between Na and SnO_2. The structure and properties of the prepared catalyst were analyzed and characterized. Subsequently, its catalytic performance was evaluated in a model ester exchange reaction. Rapeseed oil was selected as a model feedstock due to its widespread availability, moderate fatty acid composition, and relevance to industrial biodiesel production. This work aims to establish an efficient and robust catalytic pathway for sustainable biodiesel synthesis.

2. Experimental

2.1 Reagents

All reagents were employed as received without additional purification. Edible rapeseed oil, characterized by an acid value below 0.5 mg KOH/g, served as the reaction feedstock. Tin (IV) chloride pentahydrate ($SnCl_4 \cdot 5H_2O$, ≥99.0%) and sodium hydroxide (NaOH, ≥99.0%) were sourced from Sinopharm Chemical Reagent Co., Ltd. (China). Metallic sodium (Na, ≥99.0%), ammonia solution ($NH_3 \cdot H_2O$, 28–30 wt%), along with Hammett indicators including bromothymol blue, phenolphthalein, alizarin, and 2,4-dinitroaniline, were procured from Aladdin Biochemical Technology Co., Ltd. (China). Methanol (CH_3OH, ≥99.0%) and potassium hydroxide (KOH, ≥99.0%) were also obtained from Sinopharm.

2.2 Catalyst Preparation

The preparation process of the Na/SnO_2 catalyst is shown in Fig. 1. Step 1: At 60°C, a 100mL solution of 0.5mol/L $SnCl_4$ solution with a specified amount of Tween-80 was added ammonia drop by drop to adjust the pH, and the sediment was aged for 24 h. The slow addition of ammonia and the aging process are critical for controlling the nucleation and growth of SnO_2 particles, influencing their final size and morphology. The resulting sediment was then washed, filtered, and dried in 100 ◦ C for 6 h. After grinding, the sediment was calcined at different temperatures to obtain the SnO_2 support. Step2: A specific amount of SnO_2 and elemental sodium were stirred and mixed under nitrogen protection at 250 °C for 0.5 h to obtain the Na/SnO_2 solid base. The mixing temperature of 250°C was selected based on preliminary tests to ensure sufficient mobility of sodium for diffusion into the SnO_2 matrix without causing excessive volatilization or side reactions. The samples were labelled as "xwt. %Na/SnO_2" based on the mass ratio of sodium to SnO_2.

Int. Journal of Integrated Engineering Vol. 18 No. 1 (2026) p. 72-83

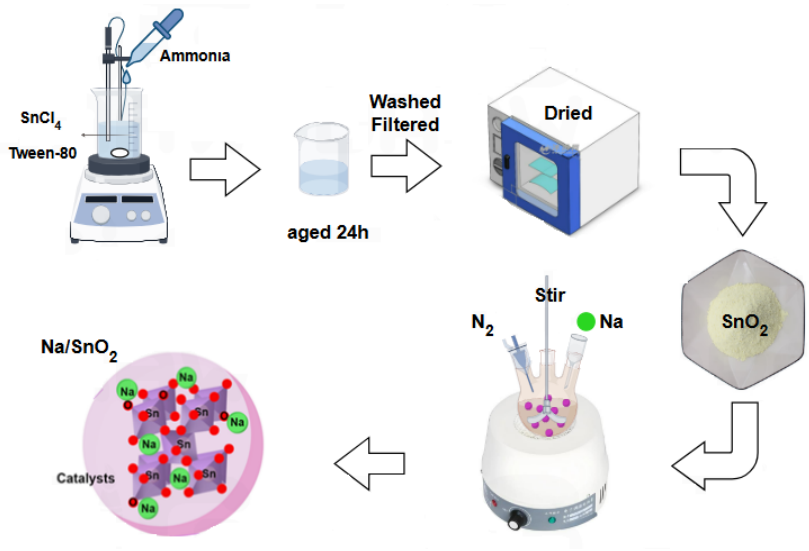

Fig. 1 *Na/SnO2 catalyst preparation process*

2.3 Catalyst Characterization

The crystalline structures of the Na/SnO_2 were examined by X-ray diffraction (XRD) using a Rigaku MiniFlex 600 diffractometer equipped with Cu Kα radiation. Measurements were conducted at 40 kV and 15 mA, scanning 2θ from 10° to 70° at a step rate of 0.02°/s. Phase identification and crystallite size estimation were performed with the JADE software, applying the Scherrer equation to the dominant diffraction peaks. Thermal behavior and stability were assessed through simultaneous thermogravimetric and differential scanning calorimetry (TG-DSC) on a TA Instruments SDT2960 analyzer. Samples were heated from ambient temperature to 800°C at 10°C/min under a continuous oxygen flow. Fourier transform infrared (FT-IR) spectra were acquired on a Shimadzu IR Affinity-1 spectrometer to probe surface functional groups and chemical bonding. Scans covered the range of 400–4000 cm^{-1} with a resolution of 4 cm^{-1}. Morphological and microstructural features were visualized using a Hitachi S-4800 field emission scanning electron microscope (FE-SEM) operated at 5 kV. The basic strength of the catalysts was evaluated via the Hammett indicator method [21]. The following indicators were utilized: bromothymol blue (pKa = 7.2), phenolphthalein (pKa = 9.3), alizarin red (pKa = 11.2), and 2,4-dinitroaniline (pKa = 15.6).

2.4 Catalyst Performance Evaluation

Catalytic activity was assessed though the transesterification reaction, as outlined in Fig. 2. Reaction Conditions: The catalyst amount was equivalent to 1% of the mass of rapeseed oil, using a methanol to rapeseed oil molar ratio (n(methanol)/n(oil)) of 6:1, at 60°C [22] for 2.5 hours. The glycerol content was determined using the saponification-periodic acid oxidation method. Glycerol content in the product mixture was quantified using a saponification–periodic acid oxidation analytical model. The average molecular weight of the rapeseed oil feedstock was approximated as 930 g/mol, derived from its typical fatty acid composition [23]. The conversion efficiency was then determined based on the theoretical and actual glycerol contents, calculated with the following expression (Equation 1):

$$Transesterification\ Conversion = \frac{R1 - R2}{R1} \times 100\% \quad (1)$$

Where:

R1: Theoretical glycerol content in raw oil

R2: Actual glycerin content in raw oil

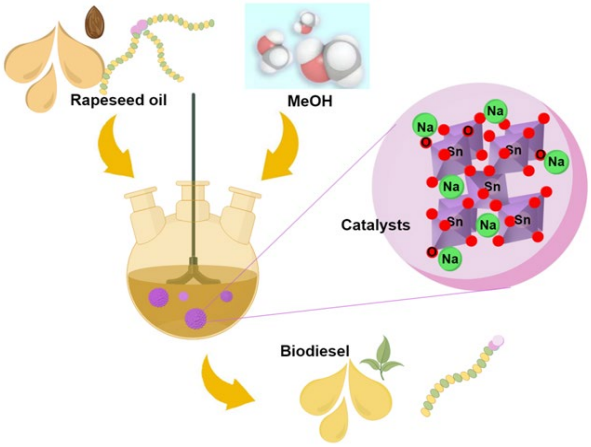

Fig. 2 *The transesterification reaction*

3. Results and Discussion

3.1 Effect of pH

As shown in Fig. 3, the conversion rate of the raw materials initially increases with pH and then decreases. When the pH reaches 8, the transesterification conversion rate peaks at 88.27%. The pH level controls the supersaturation of the solution, ultimately influencing the crystal size of the precipitate [24]. At pH < 8, insufficient supersaturation hinders effective SnO_2 crystallization and reduces the adsorption efficiency of the surfactant, thereby limiting the formation of well-defined crystalline particles. Crystallite sizes, derived from XRD data using the Debye–Scherrer equation (Table 1), decrease systematically from 1.89 nm to 1.25 nm as the pH rises from 6 to 11[25], indicating an inverse relationship between pH and SnO_2 crystallite dimension [26]. The reduction in particle size promotes improved dispersion and subsequent accessibility of sodium active sites. However, when the pH exceeds the optimum value, the crystal habit of SnO_2 undergoes a morphological transition from roughly spherical to hexagonal [26]. The stabilized crystal structure reduces the defects in the structure and improves the difficulty of mutual binding of SnO_2 and Na.

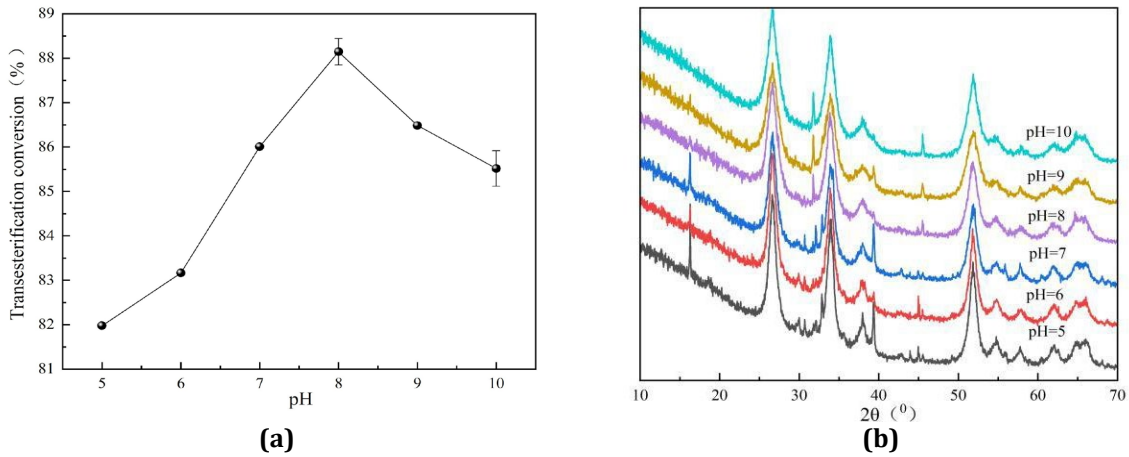

Fig. 3 *(a) Effect of the pH on the transesterification conversion; (b) XRD of catalyst samples. (Catalyst preparation conditions Calcination temperature 600 ℃; Calcination time 3h, tween-80 0.005mol, Na mass 5wt.%Na/SnO2)*

Table 1 *Grain size for different pH*

Time(h)	1	2	3	4	5	6
Grain size(nm)	1.89	1.68	1.63	1.43	1.29	1.25

Int. Journal of Integrated Engineering Vol. 18 No. 1 (2026) p. 72-83

3.2 Effect of Calcination Temperature

In Fig. 4(a), The catalytic activity of Na/SnO_2 reaches its peak when the calcination temperature reaches 600°C. Calcination temperature significantly affects the crystal structure and stability of the material. The TG curve in Fig. 4(b) indicates that the formation of SnO_2 crystals involves the gradual loss of absorbed and free water from the surface between 0-150°C [27]. Between 150-200°C, the SnO_2 weight decreases by approximately 0.2%, accompanied by a weak exothermic peak on the DSC curve due to the combustion and decomposition of the Tween surfactant, similar to Muhammad's findings [27]. From 200-500°C, the sample experiences a weight loss of about 8%, with a strong exothermic peak on the DSC curve at 500°C, indicating the reduction of surface hydroxyl groups and the transition of Sn^{2+} ions to Sn^{4+} ions, leading to the gradual formation of SnO_2 crystals [28][29]. The removal of hydroxyl groups is essential for creating a clean SnO_2 surface, which is more conducive to interaction with metallic sodium. The XRD pattern in Fig. 4(c) shows that the peaks at (220), (002), (310), (112), and (301) become increasingly distinct as the temperature exceeds 500°C, indicating enhanced crystallinity. The sharpening of these peaks confirms the growth of SnO_2 crystallites and the improvement in long-range order. However, further increasing the temperature beyond 500°C does not result in significant changes in SnO_2 mass as indicated by the TG curve, while the DSC curve still shows an endothermic process. This indicates that most structural water has been eliminated, allowing crystal grains to form and aggregate, thereby creating micropores between the grains. The formation of this porous texture is a key factor in providing accessible surface area for catalysis. This process increases the material's surface area, enhancing the contact area between the support and sodium, which subsequently improves the catalyst's activity. However, beyond 600°C, sintering and aggregation on the crystal surface may occur, resulting in a decline in catalytic performance. Sintering leads to pore collapse, a drastic reduction in surface area, and the encapsulation of active sites, all of which contribute to deactivation.

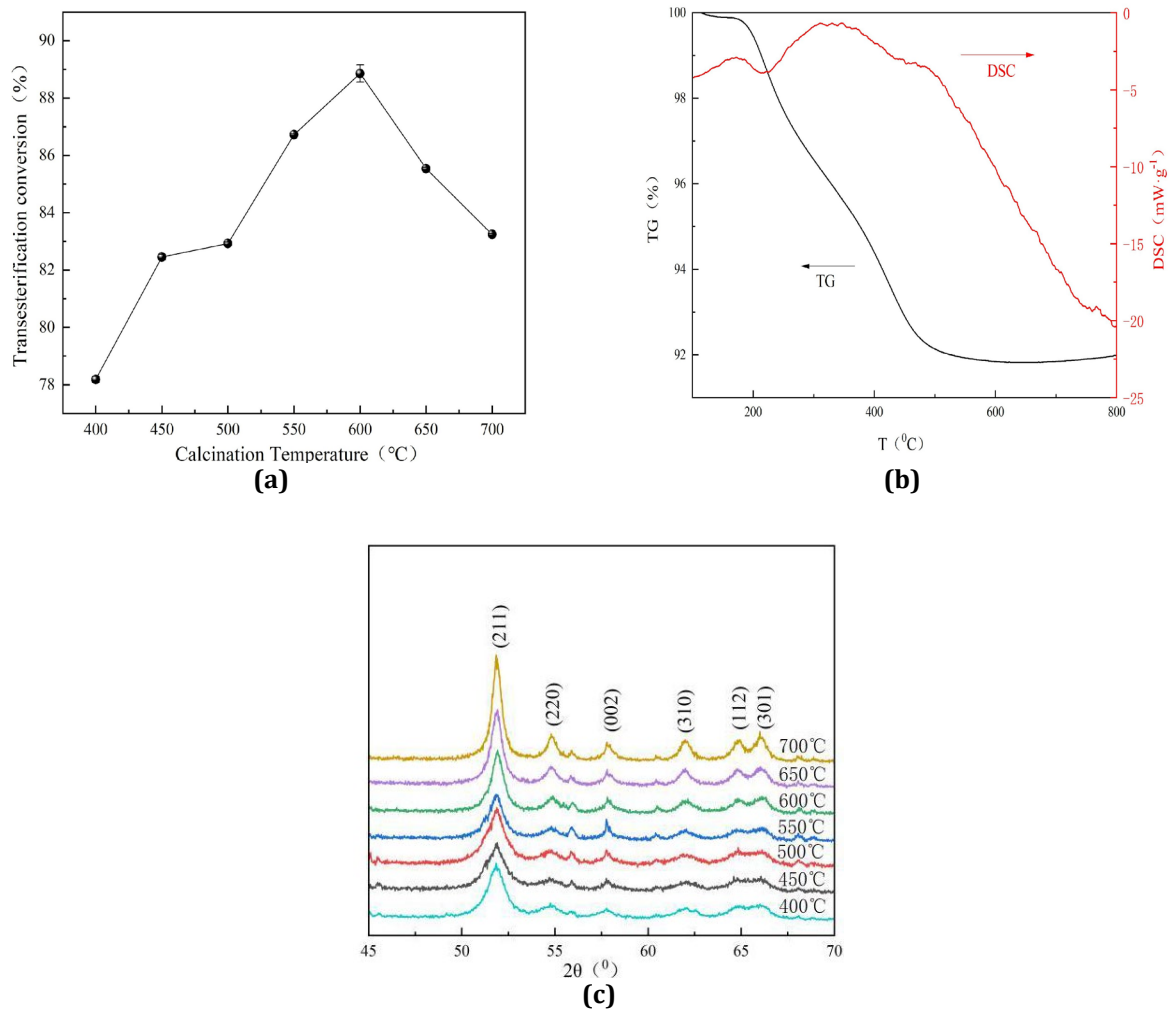

Fig. 4 *(a) Effect of the calcination temperature on the transesterification conversion; (b) TG-DSC of SnO2; (c) XRD of catalyst samples. (catalyst preparation conditions: pH=8, calcination time 3h, tween-80 0.005mol, Na mass 5wt.%Na/SnO2)*

3.3 Effect of Calcination Time

In Fig. 5(a), the catalytic activity of Na/SnO_2 initially increases with calcination time, reaching a peak conversion rate of 89.56% at the optimal calcination time of 3 h, before decreasing with further increase in time. According to the XRD patterns in Fig. 5(b), when the time of calcination is lower than 3 h, the SnO secondary phase interfaces at (002) and (112) are not fully formed [29]. The SnO phase can be attributed to the incomplete oxidation process of tin atoms. The coexistence of SnO and SnO_2 phases in the early stages of calcination creates a heterojunction interface, which may be rich in defects and active for sodium interaction. A shorter calcination time is insufficient to remove the structural water from SnO_2, thereby hindering crystal formation. However, as the calcination time increases, the SnO phase formation concurrently creates oxygen vacancies. These oxygen vacancy defects facilitate the formation of active sites between the SnO_2 support and sodium. Oxygen vacancies act as electron-rich centers, promoting the adsorption and activation of methanol, a key step in transesterification. When the calcination time exceeds 3 hours, the participation of oxygen leads to the reaction between SnO and oxygen, forming more SnO_2 and increasing the crystalline. The crystal sizes for different calcination times, obtained using the Debye-Scherrer formula, are displayed in Table 2. As the calcination time extends, the SnO_2 crystal size gradually increases, with a rapid growth rate between 2 to 4 h. The increase in particle size leads to tighter packing, resulting in the aggregation of catalyst particles, which hinders the dispersion of active sites and reduces catalytic performance. Thus, the optimal calcination time of 3 h achieves a balance between creating sufficient active defects (via controlled SnO presence and oxygen vacancies) and preventing excessive crystal growth and aggregation.

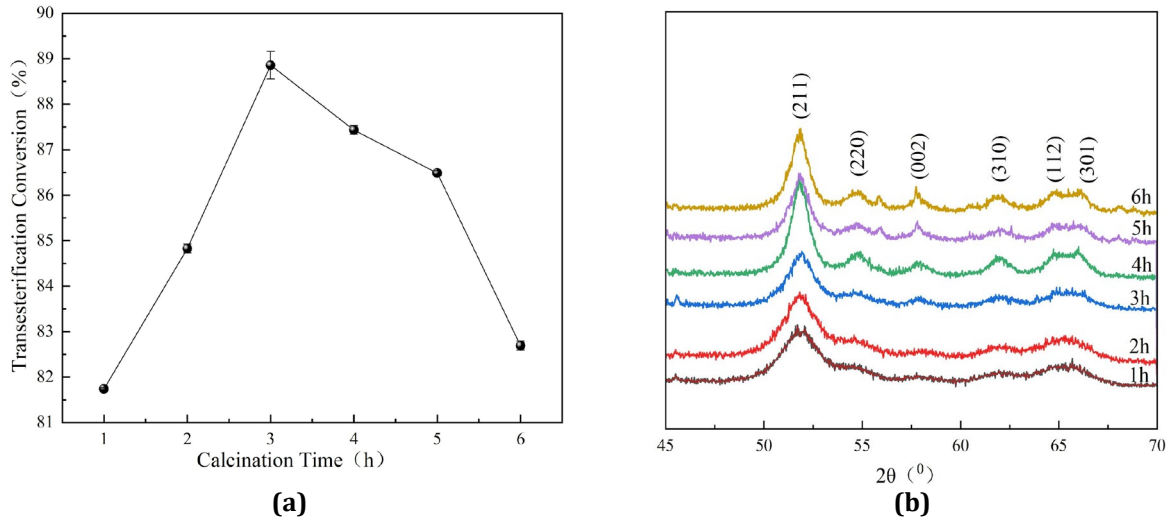

Fig. 5 *(a) Effect of calcination time on the transesterification conversion; (b) xrd of catalyst samples (catalyst preparation conditions pH=8, calcination temperature 600 ℃, tween-80 0.005mol, Na mass 5wt.%Na/SnO2)*

Table 2 *Grain size for different pH*

Time(h)	1	2	3	4	5	6
Grain size(nm)	1.074	1.105	1.336	1.735	1.755	1.765

3.4 Effect of Surfactant Amount

The conversion rate of the raw material reaches an optimal 92.4% when the surfactant concentration during catalyst preparation is 0.015 mol in Fig. 6. Beyond this concentration, the conversion rate of the transesterification reaction begins to decline. The nonionic surfactant Tween-80 facilitates the directional formation of SnO_2, effectively preventing the generation of non-framework SnO_2. Tween-80, with its hydrophilic polyoxymethylene chains and hydrophobic oleic acid tail, adsorbs onto growing SnO_2 nuclei, modifying surface energy and controlling growth kinetics. This results in a surface rich in organic groups and oxygen vacancies. An appropriate amount of Tween-80 forms a dense molecular layer covering the particle surface, effectively preventing the grains from coming into each other, resulting in smaller, well-dispersed particles [30]. However, when the Tween-80 concentration exceeds 0.015 mol, the excess molecules act as spatial fillers, diminishing the surfactant's effectiveness in directing SnO_2 formation. Consequently, a portion of the non-framework SnO_2 precipitates out,

Int. Journal of Integrated Engineering Vol. 18 No. 1 (2026) p. 72-83

leading to poorer particle dispersion and decreases the catalytic performance of the catalyst. Furthermore, excess organic residue from the surfactant requires more severe calcination for complete removal, potentially damaging the SnO_2 structure.

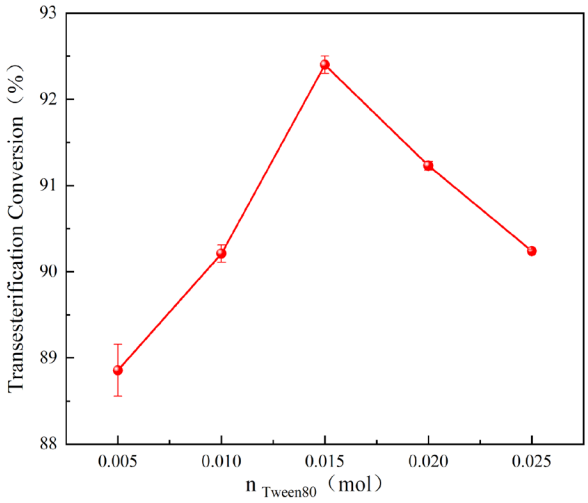

Fig. 6 *Effect of surfactant dosage on the transesterification conversion (Catalyst preparation conditions pH=8, Calcination time 3h, Calcination temperature 600 ℃, Na mass 5wt.%Na/SnO2)*

3.5 Effect of Na Loading

As depicted in Fig. 7(a), The Na/SnO_2 catalyst activity exhibits an initial increase with rising Na loading, reaching a peak conversion rate of 93.60% at 3.75 wt.% Na. Beyond this optimal loading, the catalytic activity declines. In Fig.7(b), the ◇ symbols represent the characteristic peaks of SnO_2, appearing at 26.9°, 34.2°, 38.3°, 52.2°, and 65.8° (JCPDS No. 046-1088). Notably, with increasing Na loading, no distinct peaks for metallic Na are detected, suggesting that Na reacts with SnO_2 during the loading process to form other compounds. This indicates that the synthesis method successfully promotes the reaction and incorporation of Na into the SnO_2 structure rather than merely depositing it as a separate metallic phase. Additionally, any exposed metallic Na undergoes oxidation, as evidenced by the appearance of characteristic peaks for NaOH (*), which become increasingly pronounced with higher Na loading (JCPDS No. 027-0711). This suggests that metallic Na interacts with the surface hydroxyl groups of SnO_2 or with environmental moisture, resulting in the formation of NaOH.

Furthermore, Na^+ ions are likely incorporated into surface defects of SnO_2, interacting with lattice oxygen. As shown in Fig. 7c, the prominent absorption peak at 1645 cm^{-1} is attributed to the bending vibration of adsorbed water molecules (-OH) [31]. The peak at 1375 cm^{-1} is characteristic of surface bicarbonate (HCO_3^-) species, formed by the chemisorption of atmospheric CO_2 onto basic sites [32]. This indicates the presence of basic sites on the Na_2O/SnO_2 catalyst. Meanwhile, the peak at 542 cm^{-1} may correspond to the terminal Sn-O-Sn vibration [33], while the sharp peak at 627 cm^{-1} is attributed to the stretching vibration of the Na-O bond.

However, a decline in catalytic activity is observed when the Na load exceeds 3.75 wt.%. This reduction can be attributed to the formation of sodium stannate (Na_2SnO_3) due to excess sodium., which reduces the active basic sites. The SEM image of the Na/SnO_2 catalyst calcined at 600 °C for 3 h is presented in Fig. 7d. The catalyst exhibits a relatively uniform morphology, with estimated particle sizes ranging between 1 and 5 nm, although some agglomeration is evident.

The basicity of the 3.75 wt.% Na/SnO_2 catalyst was evaluated. The catalyst causes a color change in thymol bromide (pKa = 7.2) from yellow to blue, phenolphthalein (pKa = 9.3) from light red to purple-red, and 2,4-diacetin yellow (pKa = 11.2) from yellow to red, but it does not alter the color of nitroaniline (pKa = 15.6). This result indicates that the Na/SnO2 catalyst possesses solid basicity with a basic strength between 11.2 and 15.6.

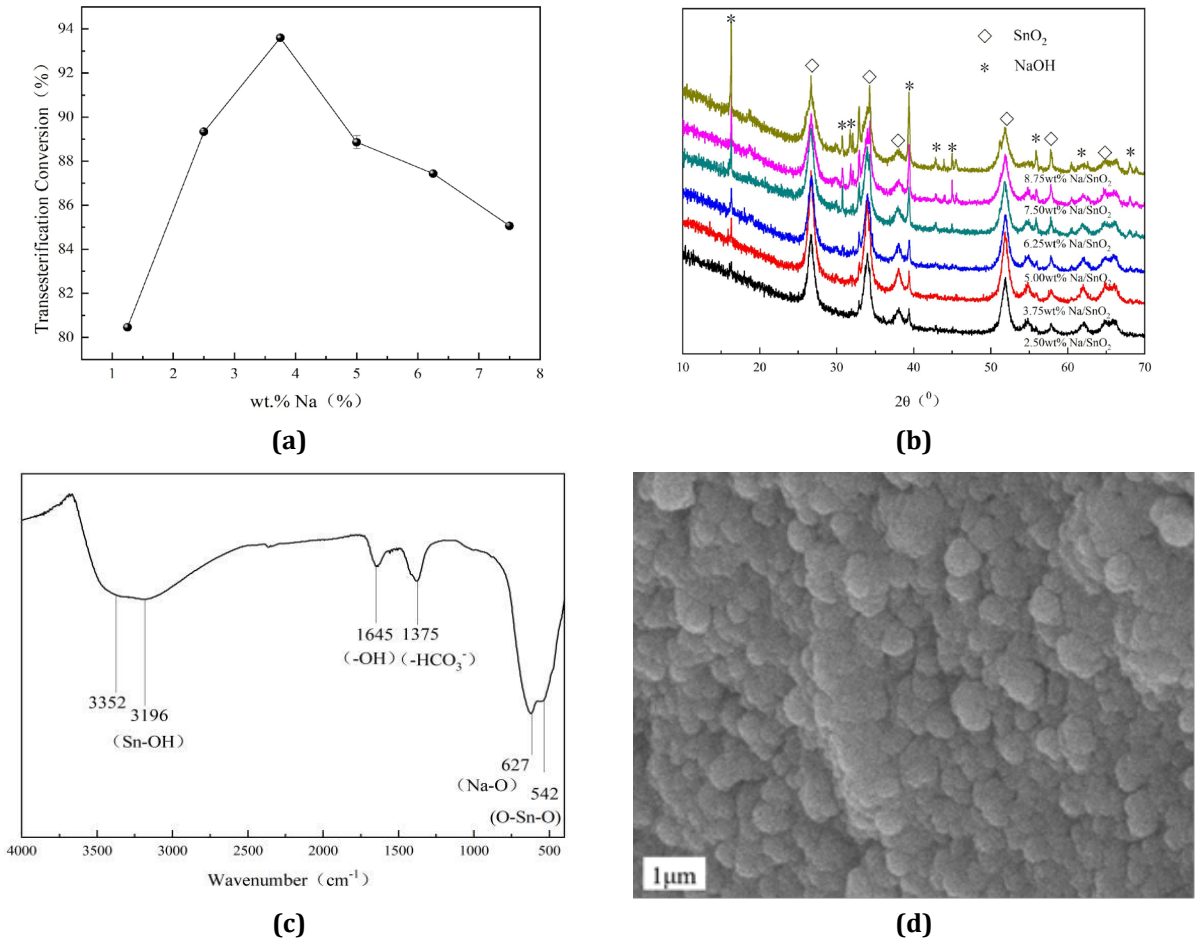

Fig. 7 *(a) Effect of the loaded sodium mass on the transesterification conversion; (b)XRD of catalyst samples; (c)FT-IR of catalyst samples; (d)SEM of catalyst samples. (Catalyst preparation conditions pH=8, Calcination time 3h, Calcination temperature 600℃, tween-80 0.005mol)*

The interaction between Na and SnO_2, which leads to the formation of basic active sites, is illustrated in Fig.8. Sodium (Na) interacts with SnO_2 in the forms of sodium hydroxide (NaOH) and sodium oxide (Na_2O). These Na species embed within the SnO_2 structure and bond with the structural oxygen, creating the active basic sites essential for catalysis. Embedding Na into the SnO_2 matrix and forming bonds with oxygen generates a significant number of basic sites, thereby enhancing the catalytic performance of the Na/SnO_2 catalyst. This interaction mechanism underscores the importance of precise Na loading to achieve optimal catalytic activity.

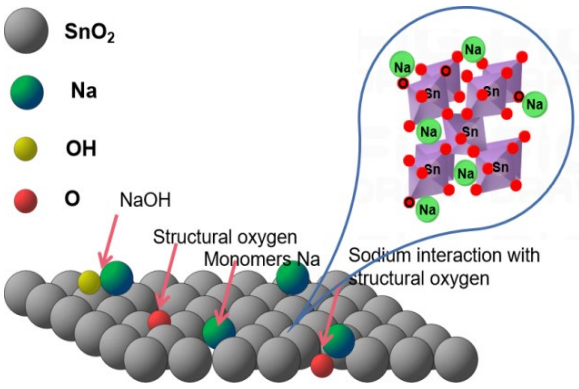

Fig. 8 *Na/SnO2 Catalyst surface mold*

Int. Journal of Integrated Engineering Vol. 18 No. 1 (2026) p. 72-83

Table 3 *Comparison of ZrO2, SnO2, CaO and MgO sources for the biodiesel production process*

Catalyst	Catalyst's preparation	Reaction conditions	Yeild(%)	Ref.
Na-ZrO_2	ZrO_2: T = 700°C, t = 3h. Na-ZrO_2: Impregnation with $NaNO_3$. Dried in 105°C for 12 hours, calcined T = 700°C,t = 3h.	[Methanol]/[oil] = 36/1, $[Catalyst]_{mass}$= 6 wt%, t = 2h T= 60°C	100%	[34]
MgO-SnO_2	SnO_2: T = 600 °C, t = 20 min. MgO-SnO_2: Dried in 100 °C for 15h, T = 600 °C, t = 2h.	[Methanol]/[oil] =9:1-21:1, $[Catalyst]_{mass}$ =1–4 wt%, t = 30–180 min, T = 40–80 °C	88%	[35]
MGO@SnO	SnO_2 : T = 600 °C, t = 2 h. MGO@SnO were sonicated for 1 h.	[Methanol]/[oil]= 10/1, $[Catalyst]_{mass}$= 5 wt%, t = 3h, T = 120°C	>88%	[36]
K/SnO_2	K/SnO_2: Dried in 100 °C for 6 h. T = 700°C, t = 5 h.	[Methanol]/[oil] = 12/1, $[Catalyst]_{mass}$ = 3 wt%, t = 1.5h, T = 65 °C	97.5%	[37]
ZnO/SnO_2	ZnO/SnO_2 : T = 500 °C, t = 2 h.	[Methanol]/[oil] = 12/1, $[Catalyst]_{mass}$ = 4 wt%, t = 2h, T = 75 °C	96.75 %.	[38]
Cage-like CaO	Cage-like CaO: T = 700°C, in N_2 atmosphere.	[Methanol]/[oil] = 15/1, $[Catalyst]_{mass}$ = 3 wt%, t = 2h, T = 65 °C	97.80 %	[39]
Na-CaO/MgO	Na-CaO/MgO: T = 900°C, t = 4h.	[Methanol]/[oil] = 12/1, $[Catalyst]_{mass}$ = 5 wt%, t = 6h, T = 65 °C	95.4%	[40]
Na/SnO_2	Na/SnO_2: T = 600°C, t = 3 hours	[Methanol]/[oil] = 6/1, $[Catalyst]_{mass}$ =1 wt%, t = 2.5h, T = 60 °C	93.6%	This work

A comparison of esterification results with various solid base catalysts is presented in Table 3. It was observed that SnO_2-based solid bases achieved relatively high esterification yields (≥88%). However, the synthesis of these catalysts typically involves a two-step process: the initial preparation of SnO_2 as a support, followed by the incorporation of active components via impregnation or mechanical mixing, and subsequent double calcination. This multistep approach increases the overall complexity and energy consumption of catalyst preparation. In contrast, although solid bases based on ZrO_2, CaO, and MgO are also commonly used, they generally require higher calcination temperatures to achieve sufficient catalytic activity.

3.6 Conclusion

In this study, a Na/SnO_2 solid base catalyst was successfully synthesized by first preparing SnO_2 via a precipitation method, followed by mixing with elemental sodium under a nitrogen atmosphere. The catalyst was evaluated for the conversion of rapeseed oil to biodiesel, with optimal preparation conditions as follows: pH 8, calcination temperature of 600 °C, calcination time of 3 hours, surfactant dosage of 0.015 mol, and sodium loading of 3.75 wt.%. Under these conditions, the transesterification rate can reach 93.6%.

This approach effectively inhibited SnO_2 dissolution and minimized alkali consumption. The resulting catalyst exhibited strong basicity, within the Hammett range of 11.2 to 15.6. Sodium interacted with SnO_2 by forming NaOH, either through bonding with surface hydroxyl groups or embedding into surface defects and reacting with lattice oxygen. While the catalyst particles were generally well-dispersed, some degree of agglomeration was

noted. Both calcination temperature and duration played critical roles in crystal development; however, excessive conditions led to sintering of active sites, thereby diminishing catalytic efficiency.

Overall, the findings present a viable strategy for synthesizing high-performance solid superbases using SnO_2 as a support. The produced biodiesel demonstrates potential for use in fuel, power generation, and other energy applications.

Building upon this work, future research will focus on the following directions: systematically evaluating the catalyst's reusability and investigating its deactivation and regeneration mechanisms; employing a combination of advanced characterization techniques and theoretical calculations to elucidate the precise structure of the active sites and the corresponding reaction mechanism. Furthermore, potential intermediates in the transesterification process will be isolated and identified to construct a more comprehensive reaction network, providing a theoretical foundation for the rational design of catalysts and the optimization of the process.

Acknowledgement

This work was supported by the Science and Technology Program (LMTD202102) and the Innovation Team Program of Liming Vocational University (PCL20061). This research is supported by the Ministry of Higher Education (MOHE) through the Fundamental Research Grant Scheme (FRGS/1/2024/TK08/UTHM/03/9).

Conflict of Interest

The authors declare that there is no conflict of interest regarding the publication of the paper.

Author Contribution

The authors confirm contribution to the paper as follows: ***study conception and design:*** *Zeng Feihu, SyYi Sim;* ***data collection:*** *Zeng Feihu;* ***analysis and interpretation of results:*** *Zeng Feihu, Wang Zhiwen, SyYi Sim;* ***draft manuscript preparation:*** *Zeng Feihu, Wang Feng. All authors reviewed the results and approved the final version of the manuscript.*

References

[1] Kalair, A., Abas, N., Saleem, M. S., Kalair, A. R., & Khan, N. (2021) Role of energy storage systems in energy transition from fossil fuels to renewables. Energy Storage, 3(1), e135. https://doi.org/10.1002/est2.135

[2] Dash RL, Mohanty B, Hota PK. (2023) Energy, Economic and environmental (3E) evaluation of a hybrid wind/biodiesel generator/tidal energy system using different energy storage devices for sustainable power supply to an Indian archipelago. Renewable Energy Focus, 44:357-372. https://doi.org/10.1016/j.ref.2023.01.004

[3] Lopresto CG. (2025) Sustainable biodiesel production from waste cooking oils for energetically independent small communities: an overview. International Journal of Environmental Science and Technology,22(3):1953-1974. https://doi.org/10.1007/s13762-024-05779-2

[4] Wang, Y.-T., Fang, Z., & Zhang, F. (2019) Esterification of oleic acid to biodiesel catalyzed by a highly acidic carbonaceous catalyst. Catalysis Today, 319, 172–181. https://doi.org/10.1016/j.cattod.2018.06.041

[5] Adewale, P., Dumont, M.-J., & Ngadi, M. (2015) Recent trends of biodiesel production from animal fat wastes and associated production techniques. Renewable and Sustainable Energy Reviews, 45, 574–588. https://doi.org/10.1016/j.rser.2015.02.039

[6] Fukuda, H., Kondo, A., & Noda, H. (2001) Biodiesel fuel production by transesterification of oils. Journal of Bioscience and Bioengineering, 92(5), 405–416. https://doi.org/10.1016/S1389-1723(01)80288-7

[7] Liu, X., He, H., Wang, Y., Zhu, S., & Piao, X. (2008) Transesterification of soybean oil to biodiesel using CaO as a solid base catalyst. Fuel, 87(2), 216–221. https://doi.org/10.1016/j.fuel.2007.04.013

[8] Sutradhar, N., Sinhamahapatra, A., Pahari, S. K., Pal, P., Bajaj, H. C., Mukhopadhyay, I., & Panda, A. B. (2011) Controlled synthesis of different morphologies of MgO and their use as solid base catalysts. The Journal of Physical Chemistry C, 115(25), 12308–12316. https://doi.org/10.1021/jp2022314

[9] Bacchiocchi, R., Ventimiglia, A., Canciani, A., Peroni, G., Tabanelli, T., Albonetti, S., Dimitratos, N., Rivalta, I., Zainal, S., & Forster, L. (2023) Structure-activity relationships of ZrO2 crystalline phases in the catalytic transfer hydrogenation of methyl levulinate with ethanol. Journal of Catalysis, 428, 115177. https://doi.org/10.1016/j.jcat.2023.115177

[10] Pérez-Madrigal, V., Ríos-Valdovinos, E., Rojas-García, E., Valenzuela, M. A., & Pola-Albores, F. (2023) Dry Reforming of Methane over Li-Doped Ni/TiO2 Catalysts: Effect of Support Basicity. Methane, 2(4), 452–469. https://doi.org/10.3390/methane2040031

[11] Wong SiewFang, W. S., Deekamwong, K., Wittakayun, J., Ling TauChuan, L. T., Muzara, O., Lee HooiLing, L. H., Adam, F., & Ng EngPoh, N. E. (2018) Nanocrystalline KF zeolite from rice husk silica as an eco-friendly solid base catalyst for the synthesis of jasminaldehyde under microwave irradiation. SAINS Malaysiana 47(02), 337-345. http://dx.doi.org/10.17576/jsm-2018-4702-16

[12] Takase, M., Kipkoech, R., Miller, D. L., & Buami, E. K. (2023) Optimisation of the reaction conditions for biodiesel from Parkia biglobosa oil via transesterification with heterogeneous clay base catalyst. Fuel Communications, 15, 100089. https://doi.org/10.1016/j.jfueco.2023.100089

[13] Liu, J., Zhang, M., & Huang, G. (2023) Conversion of Carbonaceous Organic Impurities (Methyldichlorosilane) in Trichlorosilane Using Weakly Basic Anion-Exchange Resin as Solid Catalyst. Processes, 11(2), 429. https://doi.org/10.3390/pr11020429

[14] Wang, Y., Oshima, Y., & Akizuki, M. (2024) Catalytic Performance of Solid Base Na-ZrO2 in Subcritical Water. Journal of Chemical Engineering of Japan, 57(1), 2293044. https://doi.org/10.1080/00219592.2023.2293044

[15] Xie, J., Chen, L., Au, C.-T. T., & Yin, S.-F. F. (2015) Synthesis of KOH/SnO2 solid superbases for catalytic Knoevenagel condensation. Catalysis Communications, 66, 30–33. https://doi.org/10.1016/j.catcom.2015.03.008

[16] Zhao, H., Meng, B., Wang, Y., & Zhao, S. (2025). The Synergistic Effect of Chlorine Doping and Oxygen Vacancies over SnO2 Photocatalysts for Effectively Degrading Methyl Orange. Journal of Inorganic and Organometallic Polymers and Materials, 1-13. https://doi.org/10.1007/s10904-025-03671-1

[17] Shen, C., Li, Z., Park, J. S., Li, Z., Li, C., Hong, G. H., Lee, J., Moon, H., Kim, J. M., & Jin, M. (2022) Ordered WOx/mesoporous SnO2 catalysts with excellent acetalization performance for producing bio-additives from glycerol. Molecular Catalysis, 520, 112179. https://doi.org/10.1016/j.mcat.2022.112179

[18] Liu, A., Zhu, M., & Dai, B. (2019) A novel high-performance SnO2 catalyst for oxidative desulfurization under mild conditions. Applied Catalysis A: General, 583, 117134. https://doi.org/10.1016/j.apcata.2019.117134

[19] Samart, C., Chaiya, C., & Reubroycharoen, P. (2010) Biodiesel production by methanolysis of soybean oil using calcium supported on mesoporous silica catalyst. Energy Conversion and Management, 51(7), 1428–1431. https://doi.org/10.1016/j.enconman.2010.01.017

[20] Wang, J., Zhou, D., Li, Y., & Wu, P. (2017) Experimental and first-principle studies of ferromagnetism in Na-doped SnO2 nanoparticles. Vacuum, 141, 62–67. https://doi.org/10.1016/j.vacuum.2017.03.024

[21] Xie, W., Peng, H., & Chen, L. (2006) Calcined Mg–Al hydrotalcites as solid base catalysts for methanolysis of soybean oil. Journal of Molecular Catalysis A: Chemical, 246(1), 24–32. https://doi.org/10.1016/j.molcata.2005.10.008

[22] Abbah EC, Nwandikom GI, Egwuonwu CC, Nwakuba NR. (2016) Effect of reaction temperature on the yield of biodiesel from neem seed oil. American Journal of Energy Science,3(3):16-20. http://www.openscienceonline.com/journal/energy

[23] S. M. Kosolapova, M. S. Smal, I. N. Pyagay, and V. A. Rudko (2024) The Physicochemical Basis for the Production of Rapeseed Oil Fatty Acid Esters in a Plug Flow Reactor. Processes, 12(4),788. https://doi: 10.3390/pr12040788

[24] Habte, A. G., Hone, F. G., & Dejene, F. B. (2019) The influence of malonic acid on the structural, morphological and optical properties of CdSe thin films prepared by chemical bath deposition method. Inorganic Chemistry Communications, 103, 107–112. https://doi.org/10.1016/j.inoche.2019.03.017

[25] Habte, A. G., Hone, F. G., & Dejene, F. B. (2020) Effect of solution pH on structural, optical and morphological properties of SnO2 nanoparticles. Physica B: Condensed Matter, 580, 411832. https://doi.org/10.1016/j.physb.2019.411832

[26] Sukriti, & Chand, P. (2019) Effect of pH values on the structural, optical and electrical properties of SnO2 nanostructures. In Optik, 181, 768–778. https://doi.org/10.1016/j.ijleo.2018.10.203

[27] Usman Hameed, M., Ullah Dar, S., Ali, S., Liu, S., Akram, R., Wu, Z., & Butler, I. S. (2017) Facile synthesis of low-dimensional SnO2 nanostructures: An investigation of their performance and mechanism of action as anode materials for lithium-ion batteries. Physica E: Low-Dimensional Systems and Nanostructures, 91, 119–127. https://doi.org/10.1016/j.physe.2017.04.020

[28] Jithin, P. V, Sudheendran, K., Sankaran, K. J., & Kurian, J. (2021) Influence of Fe-doping on the structural and photoluminescence properties and on the band-gap narrowing of SnO2 nanoparticles. Optical Materials, 120, 111367. https://doi.org/10.1016/j.optmat.2021.111367

[29] da Trindade, L. G., Rocha, A. C. B., Teodoro, V., da Silva, V. T., Trench, A. B., Cordoncillo, E., Teodoro, M. D., Tebcherani, S. M., Longo, E., & Mazzo, T. M. (2022) Effect of calcination temperature and pressure-assisted heat treatment on the dye degradation performance of SnO2 photocatalyst obtained by a simple synthesis method. Materials Research Bulletin, 153, 111914. https://doi.org/10.1016/j.materresbull.2022.111914

[30] Zadehnazari, A. (2024) Chemical synthesis strategies for metal oxide nanoparticles: a comprehensive review. Inorganic and Nano-Metal Chemistry, 1–40. https://doi.org/10.1080/24701556.2024.2354926

[31] Padmaja, B., Dhanapandian, S., Suthakaran, S., Ashokkumar, K., & Krishnakumar, N. (2023) Hydrothermally developed SnO2 nanoparticles and its photocatalytic degradation of Alizarin red S, Brilliant green and Methyl orange dyes and electrochemical performances. Inorganic Chemistry Communications, 149, 110363. https://doi.org/10.1016/j.inoche.2022.110363

[32] Tan, Z., Zhang, S., Zhao, F., Zhang, R., Tang, F., You, K., Luo, H., & Zhang, X. (2023) SnO2/ATP catalyst enabling energy-efficient and green amine-based CO2 capture. Chemical Engineering Journal, 453, 139801. https://doi.org/10.1016/j.cej.2022.139801

[33] Saif, N., Tariq, A., Intisar, A., Batool, Z., Arshad, M., ur Rehman, A., & Kousar, R. (2023) Green synthesis of SnO2 nanorods and Mo–SnO2 nanocomposite for efficient sun light driven organic dye photodegradation in aqueous solution. Materials Chemistry and Physics, 305, 127920. https://doi.org/10.1016/j.matchemphys.2023.127920

[34] Aguila G, Salinas D, Jiménez R, Guerrero S, Araya P. (2016) ZrO2-supported alkali metal (Li, Na, K) catalysts for biodiesel production. Journal of the Chilean Chemical Society, 61(4):3233-3238. http://dx.doi.org/10.4067/S0717-97072016000400017

[35] Velmurugan A, Warrier AR. (2022) Production of biodiesel from waste cooking oil using mesoporous MgO-SnO2 nanocomposite. Journal of Engineering and Applied Science, 69(1):92. https://doi.org/10.1186/s44147-022-00143-y

[36] Peng L, Bahadoran A, Sheidaei S, et al. (2024) Magnetic graphene oxide supported tin oxide (SnO) nanocomposite as a heterogeneous catalyst for biodiesel production from soybean oil. Renew Energy, 224:120050. https://doi.org/10.1016/j.renene.2024.120050

[37] Goudarzi F, Izadbakhsh A. (2017) Evaluation of K/SnO2 performance as a solid catalyst in the trans-esterification of a mixed plant oil. Reaction Kinetics, Mechanisms and Catalysis, 121(2):539-553. https://doi.org/10.1007/s11144-017-1176-0

[38] Yuan Z, Zhu J, Lu J, Li Y, Ding J. (2024) Preparation of biodiesel by transesterification of castor oil catalyzed by flaky halloysite supported ZnO/SnO2 heterojunction photocatalyst. Renew Energy. 227:120516. https://doi.org/10.1016/j.renene.2024.120516

[39] Huang J, Zou Y, Yaseen M, Qu H, He R, Tong Z. (2021) Fabrication of hollow cage-like CaO catalyst for the enhanced biodiesel production via transesterification of soybean oil and methanol. Fuel. 290:119799. https://doi.org/10.1016/j.fuel.2020.119799

[40] Murguía-Ortiz D, Cordova I, Manriquez ME, et al. (2021) Na-CaO/MgO dolomites used as heterogeneous catalysts in canola oil transesterification for biodiesel production. Mater Lett. 291:129587. https://doi.org/10.1016/j.matlet.2021.129587